PAIN Publish Ahead of Print
DOI: 10.1097/j.pain.0000000000001691

Spared nerve injury differentially alters parabrachial monosynaptic excitatory inputs to molecularly specific neurons in distinct subregions of central amygdala

Jun-Nan Li[1,2], Patrick L. Sheets[1,2]

[1]Department of Pharmacology and Toxicology, [2]Stark Neurosciences Research Institute, Indiana University School of Medicine, Indianapolis, IN, 46202

Address correspondence to: Patrick L. Sheets, PhD., Indiana University School of Medicine, Neuroscience Research Building 400D, 320 West 15th St, Indianapolis, IN 46202; email: plsheets@iupui.edu; phone: 317-278-6383.

Abbreviated title: Differential effects on PBn-CeA circuits after nerve injury

Number of pages including figures: 32

Number of figures: 6

Author contributions: J.L. and P.L.S designed research; J.L. performed all experiments; J.L. and P.L.S analyzed data; J.L. and P.L.S wrote the paper.

Abstract

Dissecting the organization of circuit pathways involved in pain affect is pivotal for understanding behavior associated with noxious sensory inputs. The central nucleus of amygdala (CeA) is comprised of distinct populations of inhibitory GABAergic neurons expressing a wide range of molecular markers. CeA circuits are associated with aversive learning and nociceptive responses. The CeA receives nociceptive signals directly from the parabrachial nuclei (PBn), contributing to the affective and emotional aspects of pain. While the CeA has emerged as an important node in pain processing, key questions remain regarding the specific targeting of PBn inputs to different CeA subregions and cell types. We used a multifaceted approach involving transgenic reporter mice, viral vector-mediated optogenetics, and brain slice electrophysiology to delineate cell-type-specific functional organization of the PBn-CeA pathway. Whole-cell patch clamp recordings of molecularly defined CeA neurons while optogenetically driving long-range inputs originating from PBn revealed the direct monosynaptic excitatory inputs from PBn neurons to three major subdivisions of the CeA: laterocapsular (CeC), lateral (CeL) and medial (CeM). Direct monosynaptic excitatory inputs from PBn targeted both somatostatin-expressing (SOM+) and corticotropin-releasing hormone expressing (CRH+) neurons in CeA. We find that monosynaptic PBn input is preferentially organized to molecularly specific neurons in distinct subdivisions of the CeA. The spared nerve injury model of neuropathic pain differentially altered PBn monosynaptic excitatory input to CeA neurons based on molecular identity and topographical location within the CeA. These results provide insight into the functional organization of affective pain pathways and how they are altered by chronic pain.

Key words: Parabrachial nucleus, amygdala, pain, somatostatin, corticotrophin-releasing hormone

Introduction

Pain is an unpleasant and multidimensional experience that involves sensorimotor, emotional-affective and cognitive components [54; 57]. Somatosensory pain is protective by alerting injury and/or threat [4]. However, pathological pain commonly leads to affective disorders and cognitive impairment [79; 80]. Despite progress in understanding sensory dimensions of pain, mechanisms underlying pain affect, while emerging, remain unresolved. Dissecting circuits modulating pain affect is pivotal for understanding the functional organization of neural networks mediating pain and for facilitating novel therapeutic strategies for chronic pain patients [20].

Amygdala dysfunction is implicated in many disorders including addiction, autism and anxiety disorders [18; 29; 33; 39], but it has also emerged as an important focus in pain research [57; 60]. The amygdala contains anatomically and functionally distinct nuclei: the basolateral complex, which includes the lateral (LA), basolateral (BL), and basomedial (BM) nuclei; the central nucleus (CeA), which can be subdivided into the laterocapsular (CeC), lateral (CeL) and medial (CeM) subregions [28; 48; 64]. Sensory information reaches the amygdala mainly through the LA, whereas the CeA houses major output pathways for amygdala function [48; 64]. The CeA is termed the "nociceptive amygdala" as it receives noxious sensory information from the spinal cord and brain stem via the parabrachial nucleus (PBn) [6; 9; 31; 32; 41; 57; 68; 69; 74]. Inputs from lateral PBn targeting the CeA are primarily excitatory and monosynaptic [58; 73]. Novel work has also shown that the PBn-CeA pathway transmits aversive signals important for threat and avoidance memory [17; 35; 70]. However, the organization of PBn inputs to specific neural populations in different CeA subdivisions remains unresolved.

In the BLA, a majority (≈ 80%) of neurons are glutamatergic and a minority (≈ 20%) are GABAergic [53; 72]. Conversely, the CeA houses distinct GABAergic neuronal populations expressing a wide range of molecular markers, including corticotropin-releasing hormone (CRH), somatostatin (SOM), protein kinase C-δ (PKC-δ) and neurotensin (Nts) [28; 45; 52]. Studies show that CeL-SOM+ neurons are crucial for expression of conditioned fear [49; 62] and that CeA-CRH+ neurons are involved in anxiety-like behavior and fear learning [61; 67]. Later work suggests that SOM+ and CRH+ neurons in CeL mediate appetitive, but not defensive behaviors [45]. However, organization of PB inputs to these cell types, both in naïve and chronic pain animals, remains unclear but is crucial for understanding the transition of noxious input to behavior.

Here, we used viral vector-mediated optogenetics and two transgenic Cre reporter mouse lines to selectively probe PBn inputs onto SOM+ and CRH+ neurons in distinct CeA subregions using whole-cell electrophysiological recordings in slice. These experiments expand on the notion that PBn input to the CeA is topographically organized [6; 10; 30; 41; 68] and test the hypothesis that PBn input differentially targets CeA neurons based on molecular identity. We next tested neuropathic pain-induced alterations to plasticity of PBn-CeA inputs using the spared nerve injury model (SNI). Results from our study provide insight into mechanisms of how ascending noxious inputs target specific CeA cell-types implicated in various pain-related behaviors.

Methods

Ethical Approval

The Institutional Animal Use and Care Committee of the Indiana University School of Medicine approved all procedures and experiments presented in this study. Animals were used in accordance with the animal care and use guidelines of Indiana University, the National Institutes of Health, and the Society for Neuroscience.

Animals

The heterozygous SOM-IRES-Cre;Ai14 mice were generated by mating female homozygous SOM-IRES-Cre (Jackson laboratory stock no. 013044) mice with male homozygous Ai14 (C57BL/6J-congenic version, Allen Institute line Ai14, Jackson Labs no. 007914) mice. The heterozygous CRH-ires-Cre;Ai14 mice were generated by mating female homozygous CRH-ires-Cre (Jackson laboratory stock no. 013044) mice with male homozygous Ai14 (C57BL/6J-congenic version, Allen Institute line Ai14, Jackson Labs no. 007914) mice. The heterozygous SOM-IRES-Cre;Ai14 or CRH-ires-Cre;Ai14 mice of both sexes were used in all experiments. Mice were housed on a 12:12 hour light:dark schedule (lights on at 7:00) with ad libitum access to food and water.

Intracranial injection of pACAGW-ChR2-Venus-AAV into the lateral PBn

Mice were anesthetized with 1.5% isoflurane in 100% O2 with a flow rate of 0.8 L/min (SurgiVet Isotech 4; Smith). The top of the head was shaved. The head was stabilized in a stereotaxic frame (900 series, Kopf instruments, Tujunga, CA, USA). Betadine and ethanol were applied in alternating fashion 3-4 times to disinfect the shaved area. Body temperature was maintained at 37°C using a feedback-controlled heating pad (FHC). For PBn injection, the scalp was incised, a craniotomy was made, the dura was reflected, and pipettes were advanced to reach

the stereotaxic coordinates of the desired target. The pipette was advanced to the intracranial target and a submicroliter volume (100 nL) of pACAGW-ChR2-Venus-AAV (20071-AAV1, Addgene, Watertown, MA, USA) was injected at a rate of 25 nL/min using a Hamilton syringe connected to an UltraMicoPump 3 driven by a Micro 4 MicroSyringe Pump Controller (World Precision Instruments, Sarasota, FL, USA). The pipette was kept in place for 5-7 min to limit virus reflux out of the injection site. The incision was closed with tissue adhesive (Vetbond). Following surgery, meloxicam (5 mg/kg) was injected subcutaneously for pain relief during recovery. Stereotaxic details for PBn injections are as follows: the head was fixed at a 38° down angle and coordinates were (relative to lambda): 4.42 mm caudal, 1.15 mm lateral and 3.0 mm deep at a 54° angle off the horizontal plane. Targeting of pACAGW-ChR2-Venus-AAV into the lateral PBn was verified using a fluorescence stereo microscope (Leica M165 FC) to image slices of the PBn. Animals were allowed at least 14 days of recovery and adequate anterograde ChR2-YFP expression before slice electrophysiology experiments.

Spared nerve injury model

Spared nerve injury (SNI) surgeries were performed based on published protocols from previous studies [13; 19; 23; 55]. Briefly, mice were anesthetized with 1.5% isoflurane in 100% O2 with a flow rate of 0.8 L/min (SurgiVet Isotech 4; Smith). After shaving the left hind leg area, an incision was made in the skin overlying the area where the sciatic nerve branches into 3 peripheral nerves (common peroneal, tibial and sural). The overlying muscles were spread apart to obtain access to the trifurcation of the sciatic nerve. Once exposed, the common peroneal and the tibial branches of the sciatic nerve were ligated (silk 6-0) and cut, leaving only the sural nerve intact. The wound was closed using tissue adhesive (Vetbond).

Assessment of pain behavior

Mice were acclimatized to the pain testing behavior apparatus, behavioral suite and experimenter before the von Frey filament paw-withdrawal threshold was established. Acclimatization entailed placing the mouse inside a clear 6-inch vertical plastic tube (4-inch internal diameter) on top of a wire mesh platform (exposing the hindpaws for testing). Mice were acclimatized for two non-consecutive days for 30 min each day prior to recording baseline withdrawal thresholds. Baseline withdrawal threshold (for both hindpaws) was established prior to the SNI surgery by following the 'simplified up-down' or SUDO method [11]. On postoperative day 10 (POD-10), the SUDO method was used to assess mechanical allodynia, both ipsilateral and contralateral to the injury. Experimenters were blinded to treatment groups (sham vs. SNI) during behavioral testing. Using standard von Frey filaments 2–9 (filament 1: 0.008 g; filament 2: 0.02 g; filament 3: 0.07 g; filament 4: 0.16 g; filament 5: 0.4 g; filament 6: 1 g; filament 7: 2 g; filament 8: 6 g) testing began with the middle filament (filament 4). The pressure from the filament was applied to the lateral aspect of the hind paw for 3 seconds and behavior responses such as hind paw retraction, paw licking or shaking were considered as nocifensive behavior, and classified as a pain response [51]. If the applied filament did not elicit a response the next highest filament was used, while if a response was elicited, the next lowest filament was used until the fifth and final filament was presented. This method minimized the number of filament presentations to the mouse and maximized score sensitivity. On the day of slice experiments, a final withdrawal testing was performed, with the mouse being killed immediately thereafter.

Acute brain slice preparation

After brief anesthetization by isoflurane, injected mice were decapitated and brains were rapidly extracted (< 1 min) and placed in ice-chilled cutting solution (in mM: 110 choline chloride, 25 NaHCO3 (sodium bicarbonate), 25 D-glucose, 11.6 sodium ascorbate, 7 MgSO4 (magnesium sulfate), 3.1 sodium pyruvate, 2.5 KCl, 1.25 NaH2PO4, and 0.5 CaCl2). Coronal slices (300 μm) containing the amygdala were prepared by vibratome (VT1200S, Leica), and transferred to artificial cerebrospinal solution (ACSF, in mM: 127 NaCl, 25 NaHCO3, 25 D-glucose, 2.5 KCl, 1 MgCl2, 2 CaCl2, and 1.25 NaH2PO4, aerated with 95% O2 / 5% CO2) at 37 °C for 30 min. Slices were subsequently incubated in ACSF at 21-22 °C for at least 45-60 minutes prior to electrophysiological recordings and optogenetic experiments.

Optogenetic and electrophysiological recordings

Briefly, slices were transferred to the recording chamber of a SliceScope Pro 6000 (Scientifica) containing an upright microscope (BX51, Olympus) and PatchStar micromanipulators (Scientifica), and held in place with short pieces of flattened gold wire (0.813 mm diameter; Alfa Aesar). Fluorescently labeled neurons were visualized using coolLED optics (Scientifica) and a Retiga-2000 camera (QImaging). Pipettes for whole-cell recordings were fabricated from borosilicate capillaries with filaments (G150-F, Warner) using a horizontal puller (P-97, Sutter), and filled with intracellular solution composed of the following (in mM): 128 Cs-methanesulfonate, 10 HEPES, 1 EGTA, 4 MgCl2, 4 ATP, and 0.4 GTP, 10 phosphocreatine, 3 ascorbate, and 0.05 AlexaFluor 488 (Molecular Probes), pH 7.3. EGTA was included both to facilitate seal formation and to reduce cytosolic calcium elevations induced by the various stimulus protocols used in these studies. ACSF was used as the extracellular recording solution. Recordings were targeted to tdTomato-expressing CeA neurons 60 – 100 μm deep in the slice.

Pipette capacitance was compensated; series resistance was monitored but not compensated, and required to be < 35 MΩ for inclusion in the dataset. Recordings were filtered at 4 kHz and digitized at 10 kHz. Slices were ideally used 1.5–3 h after preparation, but some were used up to 6 h after preparation. Recordings were performed at 30–34°C. The recording temperature was controlled by an in-line heating system (TC324B, Warner). The ACSF was refreshed every 2 h. In voltage clamp configuration, excitatory (glutamatergic) and inhibitory (GABAergic) responses during photoactivation of ChR2-positive PBn projections were recorded at command voltages of -70 mV (near the GABAergic reversal potential) and +10 mV (near the glutamatergic reversal potential), respectively. Wide-field photoactivation (20 msec for recording EPSCs and IPSCs, 5 msec for recording paired-pulse ratio (PPR)) of ChR2- positive PBn axons was performed using a 470 nm wavelength LED (CoolLED pE excitation system) in line with a GFP filter (ET FITC/GFP, Olympus) and a 4X objective. For isolating monosynaptic inputs, tetrodotoxin (TTX, 1 μM) and 4-aminopyridine (4-AP, 100 μM) were added to the bath solution (ACSF) at least 5 minutes before starting to record. The application of this strategy is because that the TTX abolishes action potentials and thus eliminates polysynaptic transmission relying on action potential propagation, and 4-AP blocks potassium channels and enhances local depolarization of photostimulated ChR2-expressing axons, which results in local photoevoked depolarization of presynaptic terminals sufficient to induce neurotransmitter release [63; 77]. This approach was applied in all experiments. Comparisons of monosynaptic strength were done using sequential recordings of adjacent neurons within the same brain slice and CeA subregion to limit variability due to AAV infection variability and/or slice orientation. The order of recorded neurons was alternated between paired neurons at similar depths within the slice. To evaluate the SNI-induced changes to synaptic plasticity in the PBn-CeA pathway, we used a paired-pulse

stimulation (100 msec between pulses) protocol using light to evoke transmission. The paired pulse ratio (PPR) is the ratio of the amplitude of the second EPSC to that of the first, reflecting presynaptic release probability; a lower PPR correlates with higher release probability [49].

Statistical analysis

Custom MATLAB (Mathworks, Natick, MA, USA) routines were used to analyze the data off-line. A two-way ANOVA was conducted to determine the effects of the SNI model on mechanical allodynia using Prism (GraphPad Software, San Diego, CA). For all data, a Lilliefors test was performed prior to significance testing to determine if the data were normally distributed. Comparative analyses for sequential recordings of neuron pairs were performed using the Wilcoxon Signed-Rank test. W-values represent the test statistic for the Wilcoxon Signed-Rank test. Pairwise comparisons before and after drug application were performed using the Student's paired t-test. Statistical comparisons between sham and SNI groups were performed using the Student's unpaired t-test for normally distributed data and the Wilcoxin rank-sum test for non-normally distributed data. Data are represented as means ± SEM. Significance was set at $p < 0.05$, but p-values less than 0.01 are reported.

RESULTS

Topographical expression of PBn axons overlaps with SOM+ and CRH+ CeA neurons.

To test monosynaptic input from PBn to molecularly defined neurons in distinct subregions of CeA, we injected the pACAGW-ChR2-Venus-AAV into the right lateral PBn of mice transgenically expressing TdTomato red fluorescent protein in SOM+ neurons (**Figure 1A-C**). At least two weeks after the viral delivery, acute slices containing the right CeA were prepared (**Figure 1D, E**). The expression of SOM+ neurons was detected throughout CeA with strong expression in CeL (**Figure 1F, G**). Sparse expression of SOM+ neurons was detected in

LA/BLA as previously shown [47]. We find YFP-labeled PBn axons throughout the CeA with the strongest expression in CeC (**Figure 1H, I**). However, we did not detect YFP expression in LA/BLA (**Figure 1H**). This pattern of PBn axon terminals in CeA is consistent with previous reports [27; 35; 70]. We implemented the same injection strategy in mice transgenically expressing TdTomato red fluorescent protein in CRH+ neurons (**Figure 1J-L**). In acute slices containing the CeA, robust expression of CRH+ neurons was detected within CeL with weaker expression in CeM and scarce expression in the CeC (**Figure 1M-P**). CRH+ neurons were also detected in the LA/BLA (**Figure 1P**). The pattern of PBn axon terminals in CRH-tdTomato mice was consistent with SOM-tdTomato mice (**Figure 1Q-R**). This topographic expression for SOM+ and CRH+ CeA neurons is consistent with previous studies [45; 52]. Our approach here allowed us to target molecularly defined SOM+ and CRH+ neurons in the right CeA for whole-cell recordings while optogenetically driving long-range synaptic inputs originating in PBn. We chose to target the right CeA based on compelling evidence for amygdalar lateralization in nociception [14; 15; 42; 66].

Parabrachial input differentially targets SOM+ and SOM- neurons in specific subregions of CeA

We first targeted the LA/BLA neurons as negative control for our optogenetic strategy. Wide-field photoactivation of ChR2+ PBn axons with 470 nm blue LED light did not evoke any monosynaptic EPSCs nor IPSCs (**Figure 2A, B**) in 9 BLA and 2 LA neurons, which is consistent with our anatomical results showing no YFP-labeled PBn axons in the LA/BLA region (**Figure 1**). Next, we targeted six CeA neurons (1 SOM+, 1 SOM-, 1 CRH+, 3 CRH- neurons) to measure monosynaptic EPSCs and IPSCs (**Figure 2C, D)**. Because NMDA receptors at resting membrane potential are completely blocked by Mg^{2+} [26; 44], the EPSCs measured in our

condition (1 mM Mg in ACSF and -70 mV holding membrane potential) were mediated by AMPA receptors. We observed light-evoked monosynaptic EPSCs in all 6 CeA neurons recorded, and 10 μM NBQX, an AMPA receptor antagonist, blocked the excitatory postsynaptic response in all 6 recorded neurons ($t(5) = 2.51$; $p = 0.05$; paired t-test; **Figure 2D**), confirming that the light-evoked EPSCs are AMPA-mediated.

Our recordings revealed that wide-field photoactivation of ChR2+ PBn axons with 470 nm blue LED light elicited monosynaptic EPSCs in both SOM+ and SOM- neurons recorded from all distinct subregions (CeC, CeL and CeM) of CeA (**Figure 3**). Pairs of SOM+ and SOM- CeA neurons at approximately the same depth were sequentially recorded within the same brain slice and CeA subregion to normalize for AAV infection variability and/or slice orientation (see Methods). We found no statistical difference between amplitude and paired-pulse ratio (PPR) of evoked EPSCs from recorded SOM+ (Amplitude: 100 ± 23 pA; PPR: 0.41 ± 0.04) and SOM- (Amplitude: 127 ± 38 pA; PPR: 0.41 ± 0.04) neurons in CeL (Amplitude: $W = 33$; $p = 1$; PPR: $W = 31$; $p = 0.9$, Wilcoxon Signed-Rank test; **Figure 3A-C**). In the CeC, amplitude of monosynaptic EPSCs in the SOM- neurons (325 ± 104 pA) was significantly larger than SOM+ neurons (74 ± 9.5 pA; $W = 13$; $p = 0.01$, Wilcoxon Signed-Rank test) while analysis of PPR showed no significant differences (SOM-: 0.39 ± 0.06; SOM+: 0.48 ± 0.05; $W = 35$; $p = 0.3$, Wilcoxon Signed-Rank test; **Figure 3D-F**). We detected light-evoked monosynaptic EPSCs in 12 out of 13 SOM+ and 8 out of 13 SOM- CeM neurons recorded in the CeM. Amplitude of monosynaptic EPSCs in the SOM+ CeM neurons (175 ± 53 pA) was significantly larger than EPSCs recorded in SOM- CeM neurons (64 ± 59 pA; $W = 14$; $p = 0.03$, Wilcoxon Signed-Rank test; **Figure 3G, H**), but PPR was not significantly different (SOM-: 0.49 ± 0.04; SOM+: 0.40 ± 0.06; $W = 9$; $p = 0.13$, Wilcoxon Signed-Rank test; **Figure 3I**). These data suggest that

efficiency of presynaptic glutamate release from PBn inputs does not account for differences in EPSC amplitude between SOM+ and SOM- neurons in CeL and CeM. For all PPR recordings, amplitude of monosynaptic EPSCs elicited by the second light pulse was smaller than the first light pulse indicating high release probability for PBn synapses targeting CeA neurons.

We used the same approach to test the organizational principle for monosynaptic inputs from the PBn to the CeA in the CRH-tdTomato mice. Our results showed that wide-field photoactivation of ChR2+ PBn axons elicits monosynaptic EPSCs in subsets of CRH+ and CRH- neurons recorded CeL and CeM (**Figure 4**). We did not detect expression of CRH+ neurons in CeC. We did not find any statistical differences in EPSC amplitude or PPR between CRH+ (Amplitude: 61.5 ± 16 pA; PPR: 0.30 ± 0.06) and CRH- (Amplitude: 92.1 ± 33 pA; PPR: 0.42 ± 0.07) neurons in the CeL (Amplitude: W = 33; p = 0.68; PPR: W = 7; p = 0.07, Wilcoxon Signed-Rank test; **Figure 4A-C**). Only 4 out of 8 CRH+ neurons and 5 out of 8 CRH- neurons recorded in the CeM exhibited EPSCs following stimulation of PBn inputs. As in the CeL, we did not find significant differences in EPSC amplitude or PPR between CRH+ (Amplitude: 61.5 ± 16 pA; PPR: 0.30 ± 0.06) and CRH- (Amplitude: 92.1 ± 33 pA; PPR: 0.42 ± 0.07) in CeM (Amplitude: W = 7; p = 0.3, Wilcoxon Signed-Rank test; PPR: t(7) = -0.30; p = 0.77, Student's unpaired t-test; **Figure 4G, H**).

Spared nerve injury differentially alters presynaptic release probability of parabrachial monosynaptic excitatory input to the SOM+ and SOM- neurons in distinct subregions of the CeA

We next tested whether the spared nerve injury (SNI) model of neuropathic pain alters the dynamics of PBn input to SOM+ and SOM- CeA neurons. We first injected the pACAGW-ChR2-Venus-AAV into the lateral PBn of SOM-ires-Cre;A14 mice (**Figure 5A**). Following

adequate recovery time (at least 4 days), the common peroneal and tibial nerve were cut, leaving the sural intact to establish the SNI pain model (**Figure 5B**). Pain behavior was evaluated by applying the von Frey fiber to the lateral aspect of the hind paw (**Figure 5C**). Mice undergoing the SNI surgery displayed mechanical hypersensitivity 10 days after the surgery compared to the sham mice (50% gram threshold: SNI = 0.003 ± 0.002 g; sham = 1.3 ± 0.46 g; Two-way ANOVA; $F_{1,9}$ = 6.3, p = 0.023, **Figure 5D**). In brain slices made after behavioral testing, we stimulated PBn ChR2+ axons while recording from SOM+ and SOM- neurons in distinct CeA subregions (**Figure 5E**). Our results reveal that SNI significantly increased PPR of PBn input to CeC SOM+ neurons when compared to sham mice (SNI: 0.56 ± 0.05; sham: 0.33 ± 0.05; t(10) = -2.43; *p* = 0.035, Student's unpaired t-test, **Figure 5F**). Conversely, SNI significantly reduces PPR of PBn input to CeC SOM- neurons (SNI: 0.25 ± 0.04; sham: 0.54 ± 0.06; t(11) = 3.79; *p* = 0.003, Student's unpaired t-test, **Figure 5G**). Recordings in CeL show that SNI does not alter PPR input to SOM+ (SNI: 0.46 ± 0.07; sham: 0.42 ± 0.06; t(11) = -0.415; *p* = 0.69, Student's unpaired t-test, **Figure 5H**) nor SOM- neurons (SNI: 0.47 ± 0.06; sham: 0.52 ± 0.09; t(8) = 0.461; *p* = 0.66, Student's unpaired t-test, **Figure 5I**). In CeM, our analyses showed that SNI did not alter PPR of PBn input to SOM+ neurons (SNI: 0.41 ± 0.1; sham: 0.41 ± 0.09; t(11) = 0.024; *p* = 0.98, Student's unpaired t-test, **Figure 5J**), but increased PPR of PBn input to SOM- neurons (SNI: 0.64 ± 0.11; sham: 0.31 ± 0.03; t(11) = -2.88; **p* = 0.015, Student's unpaired t-test, **Figure 5K**). These results suggest that SNI attenuates synaptic efficacy of PBn input to CeC-SOM+ and CeM-SOM- neurons while increasing synaptic efficacy of PBn input to CeC-SOM- neurons.

Spared nerve injury decreased the presynaptic release probability of parabrachial monosynaptic excitatory input to the CRH+ and CRH- CeL neurons

We next ran a set of experiments to test effects of SNI on PBn-CeA connections in CRH-ires-Cre;A14 mice (**Figure 6**). Consistent with SOM-ires-Cre;A14 mice, CRH-ires-Cre;A14 mice displayed mechanical hypersensitivity 10 days after SNI (50% gram threshold: SNI = 0.006 ± 0.002 g; sham = 0.7 ± 0.19 g; Repeated measures ANOVA; $F_{1,7}$ = 10.35, *p = 0.015; **Figure 6A**). We targeted CRH+ and CRH- neurons in distinct subregions of CeA for whole-cell patch clamp recording while optogenetically stimulating ChR2+ PBn axons (**Figure 6B**). Our results reveal that SNI significantly increases PPR of PBn inputs to both CeL CRH+ (SNI: 0.48 ± 0.05; sham: 0.26 ± 0.05; t(10) = -2.85; *p = 0.017, Student's unpaired t-test; **Figure 6C**) and CeL CRH- neurons (SNI: 0.51 ± 0.05; sham: 0.33 ± 0.02; t(25) = -2.96; **p = 0.007, Student's unpaired t-test; **Figure 6D**). However, SNI significantly reduces PPR of PBn input to CeM CRH+ neurons (SNI: 0.26 ± 0.03; sham: 0.37 ± 0.02; t(11) = 3.00; *p = 0.012, Student's unpaired t-test; **Figure 6E**). We did not observe any change of PPR in CeM CRH- neurons (SNI: 0.53 ± 0.07; sham: 0.48 ± 0.07; t(11) = 3.00; p = 0.69, Student's unpaired t-test; **Figure 6F**). These results indicate that SNI decreases the synaptic efficacy of PBn inputs targeting to CeL CRH+ and CRH- neurons while increasing the synaptic efficacy of PBn inputs targeting the CeM CRH+ neurons.

DISCUSSION

Accumulated anatomical and physiological evidence clearly demonstrates a PBn-CeA circuit that plays an essential role in the emotional-affective dimension of pain [5-8; 10; 32; 35; 57; 59; 68; 69; 76]. Excitatory synapses from PB to CeA neurons are potentiated in arthritic, visceral, neuropathic, inflammatory, and muscle pain models [34; 38; 56; 57; 59; 71; 76] and

following nociceptive stimuli with no ongoing injury [46]. These previous studies focused mainly on PBn-CeC pathways leading to the labeling of the CeC as the nociceptive-specific sub-nuclei of the CeA [12; 58; 60]. However, other reports demonstrate that the PBn-CeL pathway is also involved in nociceptive transmission [10; 25; 40]. A recent study reveals that CeL neurons expressing the calcitonin gene-related peptide receptor (CGRPR) play a key role in consolidating PBn input into threat memory [35], uncovering a molecularly specific affective pain circuit within the PBn-CeL pathway.

Here, we expand upon these findings by revealing that PBn differentially targets neurons in the CeA based on both molecular identity and topographical location within CeA. While PBn innervation of CeL and CeC subdivisions is well established, we show that PBn inputs to SOM- neurons are stronger compared to SOM+ neurons in the CeC. It is likely that CeC SOM- neurons express protein kinase C-δ (PKC-δ) based on work showing that non-overlapping PKC-δ+ and SOM+ neurons constitute 80-90% of the entire CeL/C population [36; 37; 49; 52]. This is consistent with a recent study showing greater density of CGRP+ terminals surrounding PKC-δ+ neurons compared to SOM+ neurons in CeL/C [78]. Pivotal work shows that PKC-δ+ neurons inhibit CeM output to the periaqueductal gray (PAG) [36; 49]. The PAG is a midbrain structure that integrates motivational/limbic and sensory input, including pain, to initiate specific outputs including coping behavior [2; 3; 16; 22]. Therefore, our data suggest PBn-CeC circuits preferentially and indirectly influence PAG activity, which is relevant for behavioral responses to pain input. In CeM, we show that PBn inputs to SOM+ neurons are stronger compared to SOM- neurons. While CeM projections to PAG are known [36; 49; 50], molecular profiles of these CeM-PAG neurons remain unknown. A subset of PAG-projecting neurons in CeL are SOM+ [62], but further work is needed to confirm if this is also true in CeM. Nonetheless, this

imbalanced targeting of PBn inputs suggests that SOM+ neurons play a significant role in the PBn-CeM pathway.

We find no differential targeting nor differences in synaptic efficacy of PBn input to CRH+ versus CRH- neurons in either CeL or CeM. However, probability of detecting EPSCs in CRH+ and CRH- neurons in CeL was less than observed in SOM+ and SOM- neurons. This suggests there is a small subset of CeL neurons that do not receive direct input from PBn. Only half of the CeM-CRH+ neurons produced EPSCs following stimulation of PBn inputs. This is considerably less than the probability of evoking EPSCs in CeM-SOM+ neurons, which suggests that PBn differentially targets SOM+ neurons versus CRH+ neurons in CeM. Still, current limitations of transgenic strategies does not allow us to directly compare PBn inputs to SOM+ and CRH+ neurons in CeM, which would give us the proper control for viral efficiency.

We further find that the SNI model of neuropathic pain both potentiated and attenuated the synaptic efficacy of PBn inputs to CeA neurons, as measured by paired-pulse ratio (PPR), and that the nature of these contrasting PPR changes is based on both the molecular identity of target neurons and topographical location within CeA. Amplitude of EPSCs evoked by monosynaptic inputs from PBn to late-firing CeC neurons is potentiated in the formalin model of inflammatory pain [73]. One study shows that a majority of late-firing neurons in CeL express PKC-δ [36], which suggests that inflammatory pain enhances PBn input to PKC-δ+ neurons in CeC. However, this remains unclear due to another study reporting that subpopulations of both PKC-δ+ and SOM+ neurons in CeL display a late-firing phenotype [37]. Our data show that SNI potentiates synaptic efficacy of PBn inputs targeting CeC SOM- neurons, which are likely PKC-δ+ neurons [36; 37; 49; 52]. Interestingly, we find PPR of PBn input to CeC SOM+ neurons increases after SNI, which implies an attenuated synaptic efficacy. Given the established

reciprocal inhibitory relationship between SOM+ and PKC-δ+ neurons [36; 37; 49], our observed SNI-induced decrease and increase in PPR of PBn inputs targeting CeC SOM- and CeC SOM+ neurons, respectively, suggests that neuropathic pain shifts excitatory balance toward PKC-δ+ (i.e. SOM-) neurons. Pivotal work has shown that a substantial number PKC-δ+ neurons in caudal CeL/C express the calcitonin gene-related peptide receptor (CGRPR) and that these CeL/C CGRPR+ neurons play a critical role in encoding pain input from PBn [35]. Based on these findings and our current data, we speculate that SNI evokes a long-lasting and enhanced excitatory tone to PKC-δ+/CGRPR+ neurons in CeC involving changes to synaptic plasticity of inputs from CGRP+ PBn neurons. A related study supports this notion by showing that knocking out CGRP in mice prevents decreased PPR observed in CeC neurons following induction of inflammatory pain [71]. Therefore, it is likely that we are detecting a similar PBn-CGRP effect on CeC SOM- neurons in our SNI model of neuropathic pain.

Surprisingly, we did not detect SNI-induced changes to PPR of PBn input to either CeL-SOM+ or CeL-SOM- neurons. This shows that SNI not only evokes changes to topographically distinct PBn-CeA pathways (i.e. PBn-CeC), but also induces contrasting changes to synaptic efficacy of PBn inputs based on the molecular identity of CeC neurons (i.e. SOM+ vs. SOM-). We found that SNI significantly decreases synaptic efficacy of PBn inputs targeting CeM SOM- neurons. Functions corresponding to specific molecular markers in the CeM are not well defined. Therefore, the functional significance of PPR changes to the PBn-CeM SOM- pathway following SNI is inconclusive. Nonetheless, the CeM is the major output of the CeA, and our previous data show that a significant subpopulation of CeM neurons send projections throughout multiple regions of the PAG [50] suggesting SNI may affect pain-related behaviors via a PBn-CeM-PAG pathway.

In the CeA, CRH+ neurons modulate fear- and anxiety-like behavior [1; 24; 61; 67] as well as negative effects of alcohol withdrawal [21]. We find that SNI reduced synaptic efficacy to both CRH+ and CRH- neurons in CeL, which contrasts our data showing no effects of SNI on PPR of PBn inputs to SOM+ and SOM- in CeL. One study reports negligible expression of SOM and PKC-δ in CeL-CRH+ neurons [67], while others demonstrate substantial (~70%) coexpression of SOM in CeL-CRH+ neurons [45; 52]. However, the same studies also reported that only 35-50% of CeL-SOM+ neurons express CRH [45; 52], which suggest that we did not detect effects of SNI on synaptic efficacy of PBn inputs to CeL-SOM+ neurons because a majority we recorded did not coexpress CRH. Why we see reduced synaptic efficacy to CRH- neurons in CeL is unclear. It is reported that approximately 19% of CeL neurons are CRH+ [52] meaning that the molecular heterogeneity of CeL-CRH- neurons is considerable. Approximately 90% of CeL neurons are either SOM+ or PKC-δ+, but there are a number of other molecular markers that can discriminate between CeL subpopulations including CGRPR, tachykinin 2, oxytocin receptor, neurotensin, prodynorphin and dopamine receptor 2 [35; 36; 43; 45; 52]. Our data suggest that SNI reduces synaptic efficacy of PBn input to a subpopulation of CeL-CRH- neurons that was not represented in our CeL-SOM- recordings. In CeM, we found that SNI enhances synaptic efficacy of PBn input to CRH+ neurons. The CeM contains a large number of CRH receptive neurons [67; 75], which likely respond to local release of CRH implicated in contextual memory consolidation [65]. Therefore, enhanced PBn input to CeM-CRH+ neurons may facilitate memory associated with pain following nerve injury. Whether this enhancement in synaptic efficacy happens acutely or over the development of pain behavior induced by SNI remains to be elucidated.

In summary, this study is the first to establish an organizational principle of PBn monosynaptic input to molecularly defined neurons within the three major subregions of the CeA: laterocapsular (CeC), lateral (CeL) and medial (CeM). It further establishes that plasticity of distinct PBn-CeA pathways is differentially altered in the SNI model of neuropathic pain. Together these findings provide updated insight for dissecting functional changes to CeA circuit pathways in pain models as both topography and targeting to neuronal subtypes need to be considered.

Acknowledgements: The work was funded, in part, with support from the Indiana Clinical and Translational Sciences Institute funded, in part by Award Number UL1TR002529 from the National Institutes of Health, National Center for Advancing Translational Sciences, Clinical and Translational Sciences Award. The content is solely the responsibility of the authors and does not necessarily represent the official views of the National Institutes of Health. The authors thank Brady K. Atwood for helpful comments on the manuscript.

Conflicts of interest: The authors declare no competing financial interests.

References

[1] Asok A, Draper A, Hoffman AF, Schulkin J, Lupica CR, Rosen JB. Optogenetic silencing of a corticotropin-releasing factor pathway from the central amygdala to the bed nucleus of the stria terminalis disrupts sustained fear. Molecular psychiatry 2018;23(4):914.

[2] Bandler R, Carrive P. Integrated defence reaction elicited by excitatory amino acid microinjection in the midbrain periaqueductal grey region of the unrestrained cat. Brain Res 1988;439(1-2):95-106.

[3] Bandler R, Depaulis A. Elicitation of intraspecific defence reactions in the rat from midbrain periaqueductal grey by microinjection of kainic acid, without neurotoxic effects. Neurosci Lett 1988;88(3):291-296.

[4] Basbaum A, Jessell T. The perception of pain. In: Kandel ER, Schwartz JH, Jessell TM, editors. The principles of neural science: McGraw-hill New York. p. 472-491., 2000.

[5] Bernard J, Besson J. The spino (trigemino) pontoamygdaloid pathway: electrophysiological evidence for an involvement in pain processes. Journal of neurophysiology 1990;63(3):473-490.

[6] Bernard J, Bester H, Besson J. Involvement of the spino-parabrachio-amygdaloid and-hypothalamic pathways in the autonomic and affective emotional aspects of pain. Progress in brain research, Vol. 107: Elsevier, 1996. pp. 243-255.

[7] Bernard J, Huang G, Besson J-M. The parabrachial area: electrophysiological evidence for an involvement in visceral nociceptive processes. Journal of neurophysiology 1994;71(5):1646-1660.

[8] Bernard J, Huang G, Besson J. Nucleus centralis of the amygdala and the globus pallidus ventralis: electrophysiological evidence for an involvement in pain processes. Journal of neurophysiology 1992;68(2):551-569.

[9] Bernard JF, Alden M, Besson JM. The organization of the efferent projections from the pontine parabrachial area to the amygdaloid complex: a Phaseolus vulgaris leucoagglutinin (PHA-L) study in the rat. J Comp Neurol 1993;329(2):201-229.

[10] Bernard JF, Alden M, Besson JM. The organization of the efferent projections from the pontine parabrachial area to the amygdaloid complex: a Phaseolus vulgaris

leucoagglutinin (PHA-L) study in the rat. Journal of Comparative Neurology 1993;329(2):201-229.

[11] Bonin RP, Bories C, De Koninck Y. A simplified up-down method (SUDO) for measuring mechanical nociception in rodents using von Frey filaments. Molecular pain 2014;10(1):26.

[12] Bourgeais L, Gauriau C, Bernard JF. Projections from the nociceptive area of the central nucleus of the amygdala to the forebrain: a PHA-L study in the rat. European Journal of Neuroscience 2001;14(2):229-255.

[13] Brightwell JJ, Taylor BK. Noradrenergic neurons in the locus coeruleus contribute to neuropathic pain. Neuroscience 2009;160(1):174-185.

[14] Carrasquillo Y, Gereau RWt. Activation of the extracellular signal-regulated kinase in the amygdala modulates pain perception. J Neurosci 2007;27(7):1543-1551.

[15] Carrasquillo Y, Gereau RWt. Hemispheric lateralization of a molecular signal for pain modulation in the amygdala. Molecular pain 2008;4:24.

[16] Carrive P. The periaqueductal gray and defensive behavior: functional representation and neuronal organization. Behav Brain Res 1993;58(1-2):27-47.

[17] Chiang MC, Nguyen EK, Papale AE, Ross SE. Divergent neural pathways emanating from the lateral parabrachial nucleus mediate distinct components of the pain response. bioRxiv 2019.

[18] Ciocchi S, Herry C, Grenier F, Wolff SB, Letzkus JJ, Vlachos I, Ehrlich I, Sprengel R, Deisseroth K, Stadler MB. Encoding of conditioned fear in central amygdala inhibitory circuits. Nature 2010;468(7321):277.

[19] Cooper AH, Brightwell JJ, Hedden NS, Taylor BK. The left central nucleus of the amygdala contributes to mechanical allodynia and hyperalgesia following right-sided peripheral nerve injury. Neuroscience letters 2018;684:187-192.

[20] Corder G, Ahanonu B, Grewe BF, Wang D, Schnitzer MJ, Scherrer G. An amygdalar neural ensemble that encodes the unpleasantness of pain. Science 2019;363(6424):276-281.

[21] de Guglielmo G, Kallupi M, Pomrenze MB, Crawford E, Simpson S, Schweitzer P, Koob GF, Messing RO, George O. Inactivation of a CRF-dependent amygdalofugal pathway reverses addiction-like behaviors in alcohol-dependent rats. Nat Commun 2019;10(1):1238.

[22] De Oca BM, DeCola JP, Maren S, Fanselow MS. Distinct regions of the periaqueductal gray are involved in the acquisition and expression of defensive responses. J Neurosci 1998;18(9):3426-3432.

[23] Decosterd I, Woolf CJ. Spared nerve injury: an animal model of persistent peripheral neuropathic pain. Pain 2000;87(2):149-158.

[24] Dedic N, Kühne C, Jakovcevski M, Hartmann J, Genewsky AJ, Gomes KS, Anderzhanova E, Pöhlmann ML, Chang S, Kolarz A. Chronic CRH depletion from GABAergic, long-range projection neurons in the extended amygdala reduces dopamine release and increases anxiety. Nature neuroscience 2018;21(6):803.

[25] Delaney AJ, Crane JW, Sah P. Noradrenaline modulates transmission at a central synapse by a presynaptic mechanism. Neuron 2007;56(5):880-892.

[26] Di Maio V, Ventriglia F, Santillo S. A model of cooperative effect of AMPA and NMDA receptors in glutamatergic synapses. Cognitive neurodynamics 2016;10(4):315-325.

[27] Dong YL, Fukazawa Y, Wang W, Kamasawa N, Shigemoto R. Differential postsynaptic compartments in the laterocapsular division of the central nucleus of amygdala for afferents from the parabrachial nucleus and the basolateral nucleus in the rat. Journal of Comparative Neurology 2010;518(23):4771-4791.

[28] Duvarci S, Pare D. Amygdala microcircuits controlling learned fear. Neuron 2014;82(5):966-980.

[29] Fadok JP, Krabbe S, Markovic M, Courtin J, Xu C, Massi L, Botta P, Bylund K, Müller C, Kovacevic A. A competitive inhibitory circuit for selection of active and passive fear responses. Nature 2017;542(7639):96.

[30] Fulwiler CE, Saper CB. Subnuclear organization of the efferent connections of the parabrachial nucleus in the rat. Brain Research Reviews 1984;7(3):229-259.

[31] Fulwiler CE, Saper CB. Subnuclear organization of the efferent connections of the parabrachial nucleus in the rat. Brain Res 1984;319(3):229-259.

[32] Gauriau C, Bernard J-F. Pain pathways and parabrachial circuits in the rat. Experimental physiology 2002;87(2):251-258.

[33] Gross CT, Canteras NS. The many paths to fear. Nature Reviews Neuroscience 2012;13(9):651.

[34] Han JS, Neugebauer V. Synaptic plasticity in the amygdala in a visceral pain model in rats. Neuroscience letters 2004;361(1-3):254-257.

[35] Han S, Soleiman MT, Soden ME, Zweifel LS, Palmiter RD. Elucidating an Affective Pain Circuit that Creates a Threat Memory. Cell 2015;162(2):363-374.

[36] Haubensak W, Kunwar PS, Cai H, Ciocchi S, Wall NR, Ponnusamy R, Biag J, Dong HW, Deisseroth K, Callaway EM, Fanselow MS, Luthi A, Anderson DJ. Genetic dissection of an amygdala microcircuit that gates conditioned fear. Nature 2010;468(7321):270-276.

[37] Hunt S, Sun Y, Kucukdereli H, Klein R, Sah P. Intrinsic Circuits in the Lateral Central Amygdala. eNeuro 2017;4(1).

[38] Ikeda R, Takahashi Y, Inoue K, Kato F. NMDA receptor-independent synaptic plasticity in the central amygdala in the rat model of neuropathic pain. Pain 2007;127(1-2):161-172.

[39] Janak PH, Tye KM. From circuits to behaviour in the amygdala. Nature 2015;517(7534):284.

[40] Jasmin L, Burkey AR, Card JP, Basbaum AI. Transneuronal labeling of a nociceptive pathway, the spino-(trigemino-) parabrachio-amygdaloid, in the rat. Journal of Neuroscience 1997;17(10):3751-3765.

[41] Jhamandas JH, Petrov T, Harris KH, Vu T, Krukoff TL. Parabrachial nucleus projection to the amygdala in the rat: electrophysiological and anatomical observations. Brain research bulletin 1996;39(2):115-126.

[42] Ji G, Neugebauer V. Hemispheric lateralization of pain processing by amygdala neurons. J Neurophysiol 2009;102(4):2253-2264.

[43] Jungling K, Lange MD, Szkudlarek HJ, Lesting J, Erdmann FS, Doengi M, Kugler S, Pape HC. Increased GABAergic Efficacy of Central Amygdala Projections to Neuropeptide S Neurons in the Brainstem During Fear Memory Retrieval. Neuropsychopharmacology : official publication of the American College of Neuropsychopharmacology 2015;40(12):2753-2763.

[44] Kampa BM, Clements J, Jonas P, Stuart GJ. Kinetics of Mg2+ unblock of NMDA receptors: implications for spike-timing dependent synaptic plasticity. The Journal of physiology 2004;556(2):337-345.

[45] Kim J, Zhang X, Muralidhar S, LeBlanc SA, Tonegawa S. Basolateral to central amygdala neural circuits for appetitive behaviors. Neuron 2017;93(6):1464-1479. e1465.

[46] Kissiwaa SA, Bagley EE. Central sensitization of the spino-parabrachial-amygdala pathway that outlasts a brief nociceptive stimulus. The Journal of physiology 2018;596(18):4457-4473.

[47] Krabbe S, Grundemann J, Luthi A. Amygdala Inhibitory Circuits Regulate Associative Fear Conditioning. Biological psychiatry 2018;83(10):800-809.

[48] LeDoux JE. Emotion circuits in the brain. Annu Rev Neurosci 2000;23:155-184.

[49] Li H, Penzo MA, Taniguchi H, Kopec CD, Huang ZJ, Li B. Experience-dependent modification of a central amygdala fear circuit. Nat Neurosci 2013;16(3):332-339.

[50] Li JN, Sheets PL. The central amygdala to periaqueductal gray pathway comprises intrinsically distinct neurons differentially affected in a model of inflammatory pain. J Physiol 2018.

[51] Martinov T, Mack M, Sykes A, Chatterjea D. Measuring changes in tactile sensitivity in the hind paw of mice using an electronic von Frey apparatus. Journal of visualized experiments: JoVE 2013(82).

[52] McCullough KM, Morrison FG, Hartmann J, Carlezon WA, Jr., Ressler KJ. Quantified Coexpression Analysis of Central Amygdala Subpopulations. eNeuro 2018;5(1).

[53] McDonald A. Cell types and intrinsic connections of the amygdala. The amygdala: Neurobiological aspects of emotion, memory, and mental dysfunction 1992:67-96.

[54] Merskey H. Pain terms: a list with definitions and notes on usage. Recommended by the IASP Subcommittee on Taxonomy. Pain 1979;6:249-252.

[55] Morgenweck J, Griggs R, Donahue R, Zadina JE, Taylor BK. PPARγ activation blocks development and reduces established neuropathic pain in rats. Neuropharmacology 2013;70:236-246.

[56] Nakao A, Takahashi Y, Nagase M, Ikeda R, Kato F. Role of capsaicin-sensitive C-fiber afferents in neuropathic pain-induced synaptic potentiation in the nociceptive amygdala. Molecular pain 2012;8(1):51.

[57] Neugebauer V. Amygdala pain mechanisms. Pain Control: Springer, 2015. pp. 261-284.

[58] Neugebauer V, Li W. Processing of nociceptive mechanical and thermal information in central amygdala neurons with knee-joint input. Journal of neurophysiology 2002;87(1):103-112.

[59] Neugebauer V, Li W, Bird GC, Bhave G, Gereau RW. Synaptic plasticity in the amygdala in a model of arthritic pain: differential roles of metabotropic glutamate receptors 1 and 5. Journal of neuroscience 2003;23(1):52-63.

[60] Neugebauer V, Li W, Bird GC, Han JS. The amygdala and persistent pain. The Neuroscientist : a review journal bringing neurobiology, neurology and psychiatry 2004;10(3):221-234.

[61] Paretkar T, Dimitrov E. The central amygdala corticotropin-releasing hormone (CRH) neurons modulation of anxiety-like behavior and hippocampus-dependent memory in mice. Neuroscience 2018;390:187-197.

[62] Penzo MA, Robert V, Li B. Fear Conditioning Potentiates Synaptic Transmission onto Long-Range Projection Neurons in the Lateral Subdivision of Central Amygdala. J Neurosci 2014;34(7):2432-2437.

[63] Petreanu L, Mao T, Sternson SM, Svoboda K. The subcellular organization of neocortical excitatory connections. Nature 2009;457(7233):1142.

[64] Pitkanen A, Savander V, LeDoux JE. Organization of intra-amygdaloid circuitries in the rat: an emerging framework for understanding functions of the amygdala. Trends Neurosci 1997;20(11):517-523.

[65] Pitts MW, Todorovic C, Blank T, Takahashi LK. The central nucleus of the amygdala and corticotropin-releasing factor: insights into contextual fear memory. J Neurosci 2009;29(22):7379-7388.

[66] Sadler KE, McQuaid NA, Cox AC, Behun MN, Trouten AM, Kolber BJ. Divergent functions of the left and right central amygdala in visceral nociception. Pain 2017;158(4):747-759.

[67] Sanford CA, Soden ME, Baird MA, Miller SM, Schulkin J, Palmiter RD, Clark M, Zweifel LS. A central amygdala CRF circuit facilitates learning about weak threats. Neuron 2017;93(1):164-178.

[68] Saper C, Loewy A. Efferent connections of the parabrachial nucleus in the rat. Brain research 1980;197(2):291-317.

[69] Sarhan M, Freund-Mercier MJ, Veinante P. Branching patterns of parabrachial neurons projecting to the central extended amgydala: single axonal reconstructions. Journal of Comparative Neurology 2005;491(4):418-442.

[70] Sato M, Ito M, Nagase M, Sugimura YK, Takahashi Y, Watabe AM, Kato F. The lateral parabrachial nucleus is actively involved in the acquisition of fear memory in mice. Molecular brain 2015;8(1):22.

[71] Shinohara K, Watabe AM, Nagase M, Okutsu Y, Takahashi Y, Kurihara H, Kato F. Essential role of endogenous calcitonin gene-related peptide in pain-associated plasticity in the central amygdala. European Journal of Neuroscience 2017;46(6):2149-2160.

[72] Spampanato J, Polepalli J, Sah P. Interneurons in the basolateral amygdala. Neuropharmacology 2011;60(5):765-773.

[73] Sugimura YK, Takahashi Y, Watabe AM, Kato F. Synaptic and network consequences of monosynaptic nociceptive inputs of parabrachial nucleus origin in the central amygdala. Journal of neurophysiology 2016;115(6):2721-2739.

[74] Tokita K, Inoue T, Boughter JD, Jr. Subnuclear organization of parabrachial efferents to the thalamus, amygdala and lateral hypothalamus in C57BL/6J mice: a quantitative retrograde double labeling study. Neuroscience 2010;171(1):351-365.

[75] Treweek JB, Jaferi A, Colago EE, Zhou P, Pickel VM. Electron microscopic localization of corticotropin-releasing factor (CRF) and CRF receptor in rat and mouse central nucleus of the amygdala. J Comp Neurol 2009;512(3):323-335.

[76] Veinante P, Yalcin I, Barrot M. The amygdala between sensation and affect: a role in pain. Journal of molecular psychiatry 2013;1(1):9.

[77] Yamawaki N, Suter BA, Wickersham IR, Shepherd GM. Combining optogenetics and electrophysiology to analyze projection neuron circuits. Cold Spring Harbor Protocols 2016;2016(10):pdb. prot090084.

[78] Ye J, Veinante P. Cell-type specific parallel circuits in the bed nucleus of the stria terminalis and the central nucleus of the amygdala of the mouse. Brain structure & function 2019;224(3):1067-1095.

[79] Zhuo M. Cortical excitation and chronic pain. Trends in neurosciences 2008;31(4):199-207.

[80] Zhuo M. Neural mechanisms underlying anxiety–chronic pain interactions. Trends in neurosciences 2016;39(3):136-145.

Figure legends

Figure 1. Co-expression of PBn axons and SOM+ and CRH+ CeA neurons. A, SOM-ires-CRE mice were mated with Ai14-LSL-tdTomato reporter mice to obtain SOM-ires-Cre;A14 mice. B, Delivery of pACAGW-ChR2-Venus-AAV into the PBn of SOM-ires-Cre;A14 mice. C, A representative coronal brain section showing pACAGW-ChR2-Venus-AAV injection into the right parabrachial nucleus (PBn) of a SOM-ires-Cre;A14 mouse. D, E, At least two weeks after the AAV injection, acute coronal brain slices containing the central amygdala (CeA) were prepared. F, Representative bright-field image of slice containing lateral amygdala (LA), basolateral amygdala (BLA), and subregions of the CeA (CeC: latero-capsular; CeL: lateral; CeM: medial). G, Epifluorescence image showing the expression of SOM+ neurons in the CeA. H, Epifluorescence image showing the expression of the PBn axons in the CeA. I, Merged image showing the co-expression of tdTomato- expressing SOM+ neurons and Venus-expressing PBn axons in the CeA. J, CRH-ires-CRE female mice were mated with Ai14-LSL-tdTomato reporter mice to obtain CRH-ires-Cre;A14 mice. K, Delivery of pACAGW-ChR2-Venus-AAV into the right PBn of CRH-ires-Cre;A14 mice. L, Coronal brain section showing pACAGW-ChR2-

Venus-AAV injection into the right PBn from a CRH-ires-Cre;A14 mouse. M, N, At least two weeks after the AAV injection, acute coronal brain slices containing the CeA were prepared. O, Bright-field image showing a representative acute coronal brain slice containing the CeA. P, Epifluorescence image showing the expression of CRH+ neurons in the CeA and LA/BLA. Q, Epifluorescence image showing the expression of the PBn axons in the CeA. R, Merged image showing the co-expression of CRH+ neurons and PBn axons in the CeA. L: lateral, V: ventral.

Figure 2. Photoactivation of PBn axon terminals elicited a glutamatergic monosynaptic EPSC in the CeA, but not BLA. A, Schematic of wide field stimulation of PBn axons while recording in the LA/BLA. B, Photoactivation of PBn axon terminals with blue light did not evoke glutamatergic monosynaptic EPSCs (top) nor monosynaptic IPSCs (bottom) in the LA/BLA neurons (n = 9; BLA = 7, LA = 2). C, Schematic of wide field stimulation of PBn axons while recording in the CeA. D, Photoactivation of PBn axon terminals with blue light evoked glutamatergic monosynaptic, AMPA-mediated EPSCs (top), but not IPSCs in CeA neurons (bottom). E, The AMPA receptor antagonist NBQX blocked PBn evoked EPSCs in CeA neurons (1 SOM+, 1 SOM-, 1 CRH+, 3 CRH- neurons, 4 mice, * p = 0.05).

Figure 3. Organization of parabrachial monosynaptic excitatory input to SOM+ and SOM- neurons in subdivisions of the CeA. A, Schematic recording configuration in CeL of SOM-tdTomato mice. B, Representative traces of light-evoked (blue ticks) monosynaptic EPSCs (left, at -70 mV holding potential, 1 μM TTX + 100 μM 4-AP) and PPR (right, at -70 mV holding potential, 1 μM TTX + 100 μM 4-AP; interval 100 msec) in SOM+ (red) and SOM- (black) CeL neurons. C, Comparison of monosynaptic EPSCs and paired-pulse ratio (PPR) between SOM+ and SOM- CeL neurons (n = 11 pairs/5 mice). D, Schematic recording configuration in CeC. E, Representative traces of light-evoked monosynaptic EPSCs and PPR in SOM+ and SOM- CeC

neurons. F, Comparison of monosynaptic EPSCs and paired-pulse ratio (PPR) between SOM+ and SOM- CeC neurons (n = 14 pairs/5 mice; *p < 0.05). G, Schematic recording configuration in CeM. H, Representative traces of light-evoked monosynaptic EPSCs and PPR in SOM+ and SOM- CeM neurons. I, Comparison of monosynaptic EPSCs and paired-pulse ratio (PPR) between SOM+ (red) and SOM- (black) CeC neurons (n = 14 pairs/5 mice; *p < 0.05). Pairs are connected by lines; mean ± S.E.M. of SOM- values (normalized to SOM+ pair) is plotted to the right. Comparison of the monosynaptic EPSCs and PPR between SOM+ and SOM- CeM neurons (n = 14 EPSC pairs; 9 PPR pairs / 5 mice; *p < 0.05).

Figure 4. Organization of parabrachial monosynaptic excitatory input to the CRH+ and CRH- neurons in subdivisions of the CeA. A, Schematic recording configuration in CeL of CRH-tdTomato mice. B, Representative traces of light-evoked monosynaptic EPSCs and PPR (interval 100 msec) recorded from a CRH+ (red) and CRH- (black) CeL neurons. C, Comparison of monosynaptic EPSCs ($t(11) = -1.05$; $p = 0.32$, Student's paired t test) and PPR ($t(6) = -1.84$; $p = 0.11$, Student's paired t test) between CRH+ and CRH- CeL neurons (n = 12 EPSC pairs; 7 PPR pairs / 5 mice). D, Schematic recording configuration in CeM of CRH Cre mice. F, Representative traces of light-evoked monosynaptic EPSCs and PPR (interval 100 msec) recorded from a CRH+ (red) and CRH- (black) CeM neuron. G, Comparison of monosynaptic EPSCs ($t(7) = -1.23$; $p = 0.26$, Student's paired t-test) and PPR (CRH+: 4; CRH-: 5; $t(7) = -0.30$; $p = 0.77$, Student's unpaired t-test) between CRH+ and CRH- CeM neurons (n = 8 EPSC pairs / 5 mice).

Figure 5. SNI distinctly alters PBn input to SOM+ and SOM- neurons based on subdivision of CeA. A, Delivery of pACAGW-ChR2-Venus-AAV into the PBn of SOM-ires-Cre;A14 mice. B, Schematic of SNI surgery involving transection (grey line) of the tibial and peroneal branches of

the sciatic nerve, leaving the sural nerve intact. C, SNI and sham-operated mice were placed in cages on an elevated mesh platform for assessment of pain behavior using von Frey filaments. The hind paw region innervated by the sural nerve (red) skin was targeted the von Frey hair while regions innervated by common peroneal (black) and tibial (grey) nerve were avoided. D, 50% withdrawal threshold response (mean ± SEM) to von Frey fibers of SNI (n = 5) and sham (n = 5) mice (*p = 0.023) on post-operative day 10 (POD-10). E, SOM+ and SOM- CeA neurons were sequentially recorded during blue (470 nm) LED wide-field stimulation of ChR2-expressing PBn axons. F, Representative traces (top) and statistical comparison (bottom) of PPR in SOM+ CeC neurons from SNI mice compared to sham mice (SNI: 6 neurons; Sham: 6 neurons; *p = 0.035). G, Representative traces (top) and statistical comparison (bottom) of PPR in SOM- CeC neurons from SNI mice compared to sham mice (SNI: 6 neurons; Sham: 7 neurons; **p = 0.003). H, Representative traces (top) and statistical comparison (bottom) of PPR in SOM+ CeL neurons from SNI and sham mice (SNI: 7 neurons; Sham: 6 neurons; p = 0.69). I, Representative traces (top) and statistical comparison (bottom) of PPR in SOM- CeL neurons from SNI and sham mice (SNI: 5 neurons; Sham: 5 neurons; p = 0.66). J, Representative traces (top) and statistical comparison (bottom) of PPR in SOM+ CeM neurons from SNI mice and sham mice (SNI: 6 neurons; Sham: 7 neurons; p = 0.98). K, Representative traces (top) and statistical comparison (bottom) of PPR in SOM- CeM neurons from SNI mice compared to sham mice (SNI: 6 neurons; Sham: 7 neurons; t(11) = -2.88; *p = 0.015, Student's unpaired t-test).

Figure 6. SNI differentially alters PBn input to CRH+ and CRH- neurons in distinct subregions of CeA. A, 50% withdrawal threshold response (mean ± SEM) to von Frey fibers of SNI (n = 5) and sham (n =4) mice (*p = 0.015) on post-operative day 10 (POD-10). B, CRH+ and CRH- CeA neurons were recorded during blue (470 nm) LED wide-field stimulation of ChR2-

expressing PBn axons. C, Representative traces (top) and statistical comparison (bottom) of PPR in CRH+ CeL neurons from SNI compared to sham mice (SNI: 7 neurons; Sham: 5 neurons; *p = 0.017). D, Representative traces (top) and statistical comparison (bottom) of PPR in CRH- CeL neurons in the SNI mice (SNI: 14 neurons; Sham: 13 neurons; **p = 0.007). E, Representative traces (top) and statistical comparison (bottom) of PPR in CRH+ CeM neurons in SNI compared to sham mice (SNI: 5 neurons; Sham: 8 neurons; *p = 0.012). F, Representative traces (top) and statistical comparison (bottom) of PPR in CRH- CeM neurons between SNI and sham mice (SNI: 9 neurons; Sham: 10 neurons; p = 0.69).

FIGURE 1

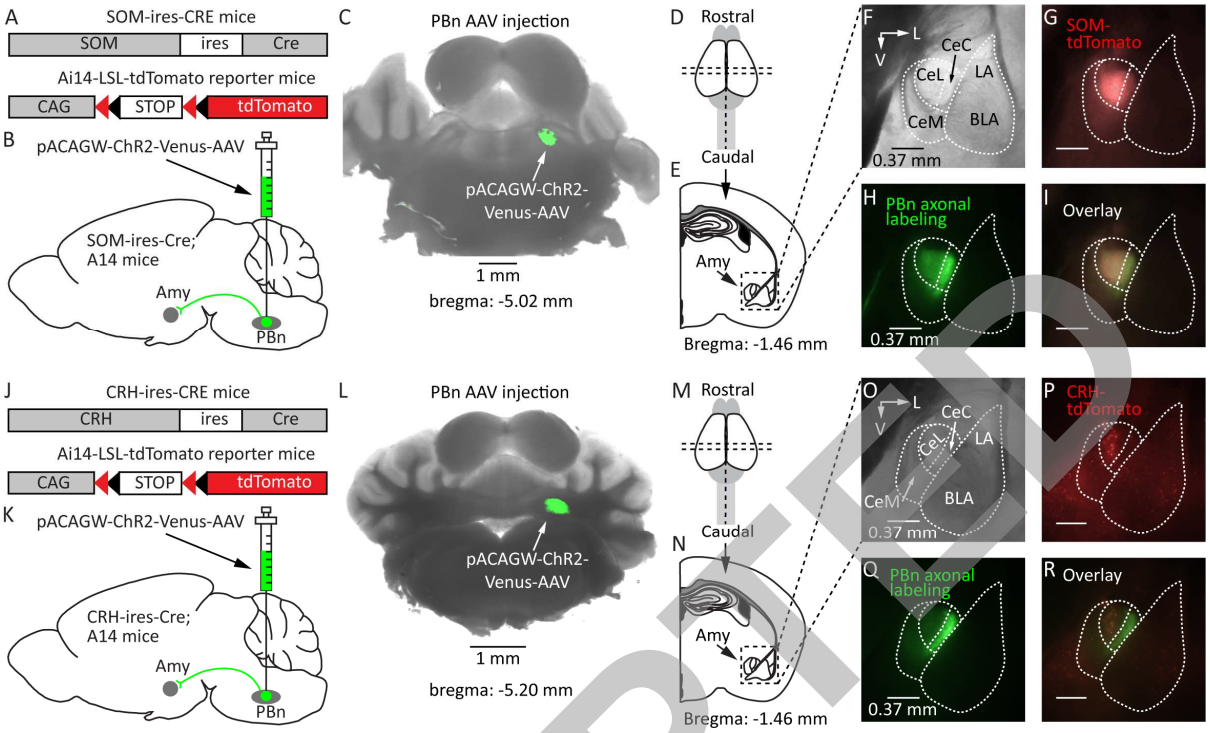

FIGURE 2

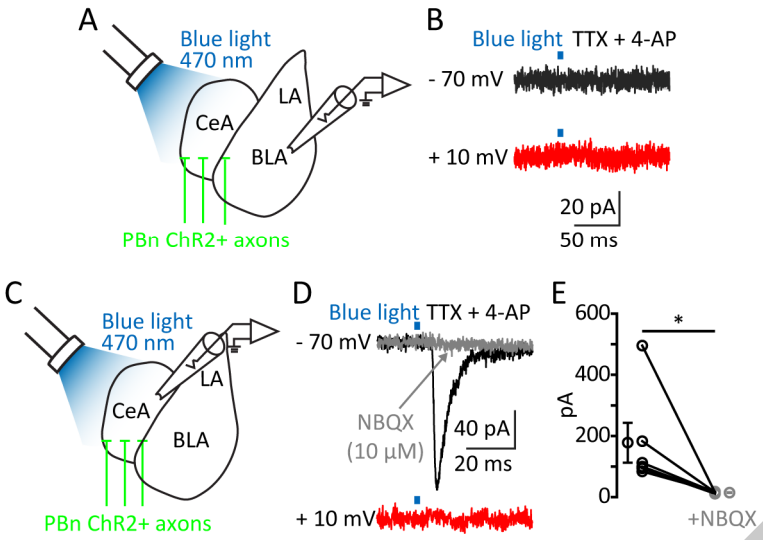

FIGURE 3

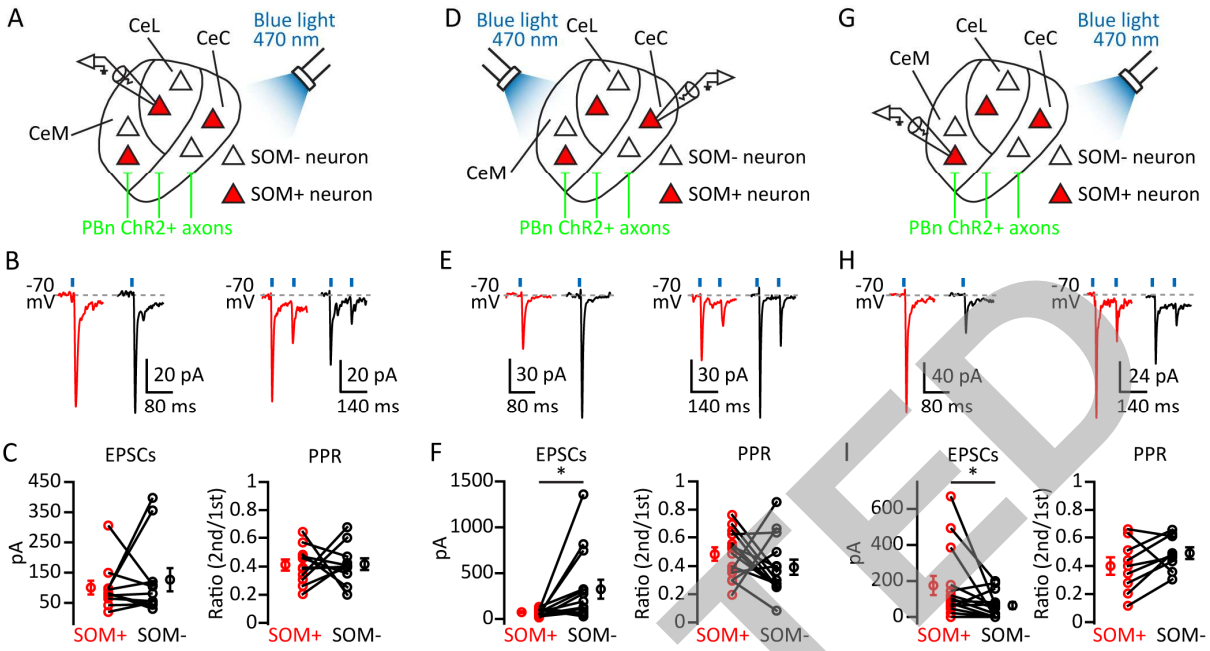

FIGURE 4

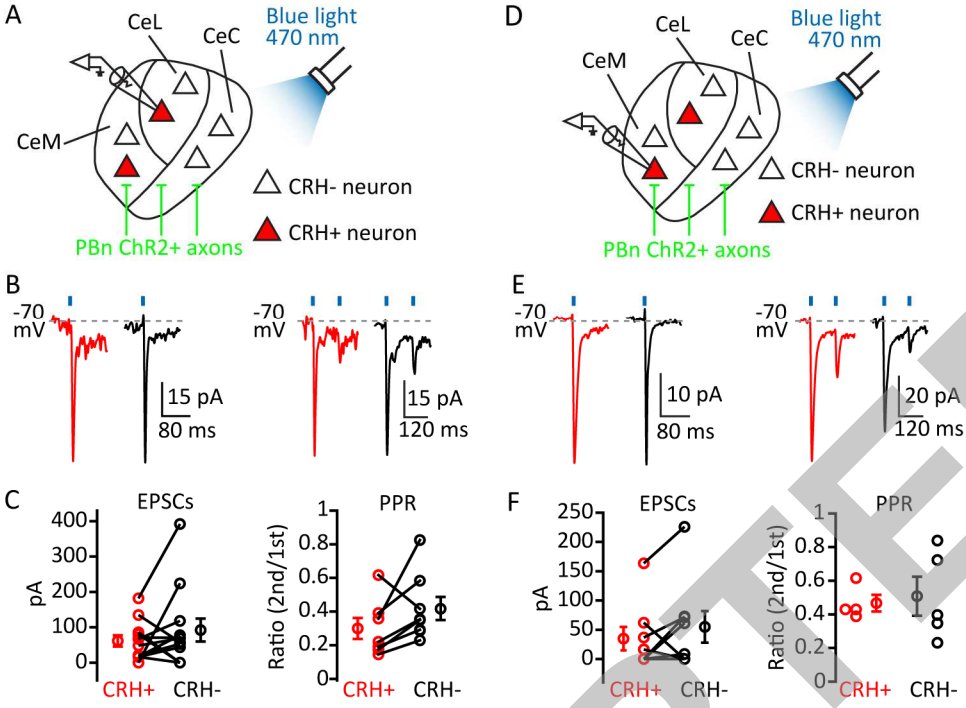

FIGURE 5

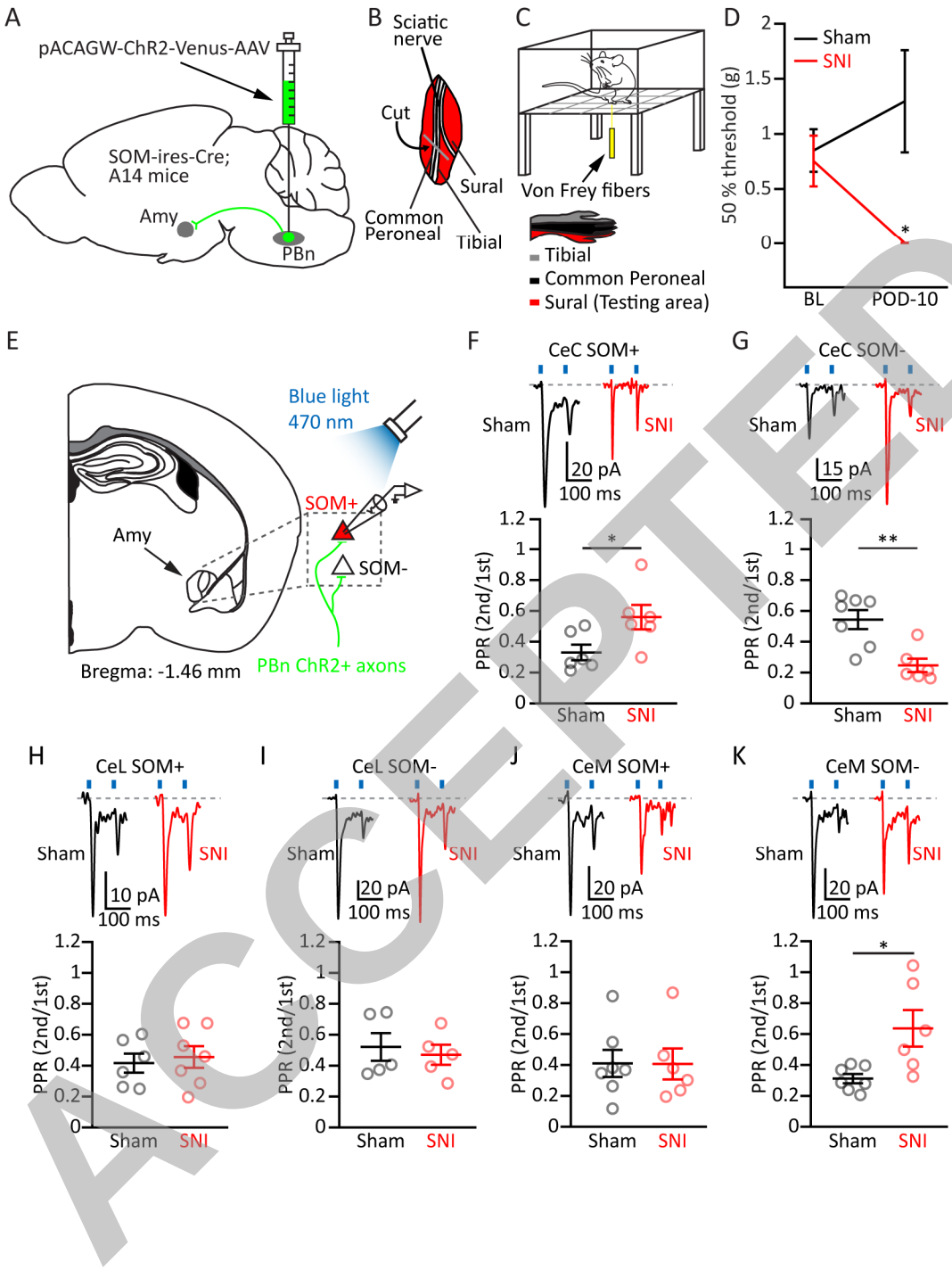

FIGURE 6